PHYSICAL REVIEW B **87**, 014502 (2013)

Optical study of superconducting Ga-rich layers in silicon

T. Fischer,* A. V. Pronin,† R. Skrotzki, T. Herrmannsdörfer, and J. Wosnitza
Dresden High Magnetic Field Laboratory (HLD), Helmholtz-Zentrum Dresden-Rossendorf, 01314 Dresden, Germany

J. Fiedler, V. Heera, and M. Helm
Institute of Ion Beam Physics and Materials Research, Helmholtz-Zentrum Dresden-Rossendorf, 01314 Dresden, Germany

E. Schachinger
Institute of Theoretical and Computational Physics, Graz University of Technology, 8010 Graz, Austria
(Received 12 June 2012; revised manuscript received 18 November 2012; published 2 January 2013)

We performed phase-sensitive terahertz (0.12–1.2 THz) transmission measurements of Ga-enriched layers in silicon. Below the superconducting transition $T_c^{\text{middle}} = 6.7$ K we find clear signatures of the formation of a superconducting condensate and of the opening of an energy gap in the optical spectra. The London penetration depth $\lambda(T)$ and the condensate density $n_s = \lambda^2(0)/\lambda^2(T)$ as functions of temperature demonstrate behavior typical for conventional superconductors with $\lambda(0) = 1.8\ \mu$m. The terahertz spectra can be well described within the framework of Eliashberg theory with strong electron-phonon coupling: the zero-temperature energy gap is $2\Delta(0) = 2.64$ meV and $2\Delta(0)/k_BT_c = 4.6$, consistent with the amorphous state of Ga. At temperatures just above T_c, the optical spectra demonstrate Drude behavior.

DOI: 10.1103/PhysRevB.87.014502 PACS number(s): 74.25.Gz, 74.70.Ad, 74.78.−w, 74.25.nd

I. INTRODUCTION

Recently, some of us observed superconductivity in Ga-enriched layers manufactured by Ga implantation into Si wafers and subsequent thermal annealing.[1] These layers consist of amorphous, gallium-rich precipitates embedded in nanocrystalline silicon.[2] Compared to ordinary bulk crystalline gallium with $T_c = 1.1$ K, superconductivity in its amorphous modification is known to occur at higher temperatures, typically $T_c = 6$–8.5 K.[3–5] Tunneling, microwave, and infrared measurements of amorphous Ga have proven it is a strong-coupling superconductor with $2\Delta(0)/k_BT_c = 4.2$–4.5.[6–14] In the Ga layers in Si, the superconducting transition occurs at comparable temperatures with the onset at 7–10 K. However, differently from other amorphous Ga films, these samples withstand multiple cooling procedures and room-temperature handling,[1,2] making them interesting for potential applications.

Here, we report an optical (terahertz) study of the gallium-enriched layers in silicon. Optical spectra of superconductors contain valuable information about the superconducting state: the London penetration depth, the strength of coupling, the size and the symmetry of the superconducting gap can be extracted from such measurements.[15,16] In our optical measurements, we observe clear signatures of the superconducting-state formation at $T < T_c$. We were able to trace the temperature dependence of the spectral weight of the superconducting condensate and of the London penetration depth. We demonstrate that they nicely follow the behavior expected for fully gapped superconductors. Further, we estimate the superconducting energy gap from our optical measurements and show that the frequency-dependent optical spectra can be well described within the Eliashberg theory for strong-coupling s-wave superconductors.

II. EXPERIMENT

Ga^+ ions had been implanted at an energy of 80 keV with a total fluence of 4×10^{16} cm^{-2} Ga into 0.38-mm-thick (100)-oriented silicon wafers covered with 30 nm of silicon dioxide. Subsequent rapid thermal annealing at 650 °C for 60 s has been applied for realizing gallium precipitation at the Si-SiO_2 interface. The thickness of the fabricated Ga-rich layers was estimated to be 10 nm by means of transmission electron microscopy and Rutherford backscattering.[2] The samples probed optically had lateral sizes of 2×5 mm. Direct-current resistivity measurements (Fig. 2) show the onset of the superconducting transition at $T_c^{\text{onset}} \approx 7.3$ K and a middle point at $T_c^{\text{middle}} = 6.7$ K, which we take as T_c for our Eliashberg analysis below. Further information, such as a detailed structural and critical-field analysis, can be found in Refs. 1 and 2.

In the frequency range 3.9–41 cm^{-1} (117–1230 GHz, 0.48–5.1 meV), measurements have been performed by use of a spectrometer, equipped with backward-wave oscillators (BWOs) as sources of coherent and frequency-tunable radiation, which propagates in free space. A diagram of the spectrometer is shown in Fig. 1. The measurements have been performed using a number of different BWOs covering the above-mentioned frequency range almost continuously. A Mach-Zehnder interferometer arrangement of the spectrometer allows one to measure both the intensity and the phase shift of the wave transmitted through the sample (for the transmittance measurements, the reference arm of the interferometer is blocked with a shutter). Freestanding wire grids are used as the beam splitter and beam combiner of the interferometer. The beam-splitter wire grid also sets the polarization of the light incident on the sample. Additional grids are used for balancing intensities in the interferometer arms.

A commercial optical ^{4}He cryostat with the sample inside is installed in one of the arms of the interferometer. A custom-made sample holder allows accurate up-and-down movement of the sample behind a metallic aperture in such a way that the sample can be taken out of the beam path for empty-channel measurements and introduced back into the beam with high reproducibility of its position. Two successive measurements

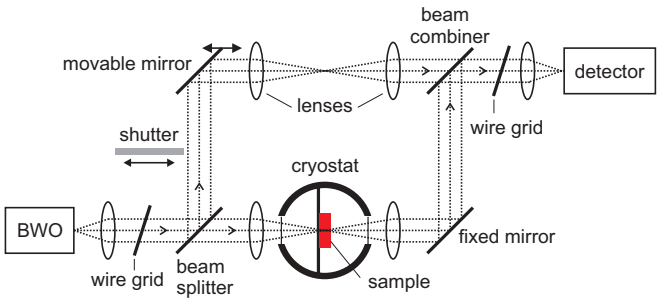

FIG. 1. (Color online) Diagram of the spectrometer used for optical measurements at (sub)terahertz frequencies. BWOs are used as radiation sources.

of the sample after such an up-and-down move reproduce each other with accuracy better than 1% in both transmittance and phase-shift modes.

A mirror in another (reference) arm of the interferometer is connected to a precision stepper motor (with an accuracy of 0.5 μm). The interferometer can be adjusted to a position where the optical path difference between the arms is zero. During frequency or temperature sweeps, a software always keeps the movable mirror in position with zero optical path difference. Any change in the sample's refraction index (or dielectric permittivity) results in a change of the optical path length in the sample arm, and, hence, to a shift of the movable mirror. This shift is detected and the phase change of the wave transmitted through the sample is directly calculated from it.

The absolute values of the sample's transmittance and transmission phase shift, Tr and φ, are obtained by repeating the measurements without a sample and a subsequent correction for the empty-channel measurement. Fresnel optical formulas[17] are used to extract the optical parameters of the sample (for example, the complex conductivity $\sigma = \sigma_1 + i\sigma_2$, or the complex permittivity $\varepsilon = \varepsilon' + i\varepsilon''$) from Tr and φ.

A general description of the measurement technique can be found in Refs. 18 and 19. This method has been previously

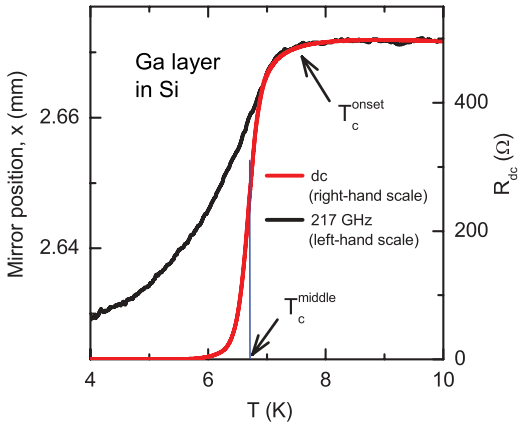

FIG. 2. (Color online) Temperature dependence of the resistance of a Ga-enriched layer in Si (right-hand scale) and an example of the raw measurements of the interferometer mirror position (left-hand scale). The mirror position is directly related to the optical phase shift and, hence, to the permittivity and the penetration depth.

applied to a large number of different materials, including films of different superconductors (see, for example, Refs. 20–24).

The London penetration depth $\lambda = c/(4\pi\sigma_2\omega)^{1/2}$ (ω is the angular frequency, c is the speed of light), has been determined as a function of temperature at a number of fixed frequencies (123, 172, 217, and 252 GHz, or 4.1, 5.74, 7.24, and 8.4 cm^{-1}) in the same way as described in Refs. 23 and 24. For these measurements, we limited ourselves to our lowest frequencies, as at higher frequencies the contribution of normal electrons to σ_2 becomes significant, thus, a correct determination of λ is difficult.

The optical parameters of pristine wafers had been measured in advance using the same setup. At $T \leqslant 15$ K, we found the real part of the dielectric permittivity of the wafers to be independent of temperature and frequency (within our accuracy) and equal to $\varepsilon' = 11.50 \pm 0.05$. An absorption in the wafers was not detectable at these temperatures. We have found that neither silicon wafers nor our sample demonstrate any in-plane optical anisotropy.

III. RESULTS AND DISCUSSION

A. Temperature sweeps: Temperature dependence of penetration depth and condensate density

First, let us note that the appearance of superconductivity in our sample is confirmed by the raw optical data. In Fig. 2, we show an example of such raw data—the position of the movable mirror of the Mach-Zehnder interferometer $x(T)$ as a function of temperature. Above the superconducting transition, $x(T)$ is flat. As the sample enters into the superconducting state, $x(T)$ starts to decrease rapidly. This is due to the condensation of electrons and the superconducting gap opening.

The condensed electrons are represented by a δ function in the real part of the complex conductivity, σ_1. This δ function leads (via the Kramers-Kronig relations) to a divergence in σ_2 (and in ε') at $\omega \to 0$: $\sigma_2 = ne^2/m\omega$, $\varepsilon' \equiv 1 - 4\pi\sigma_2/\omega = 1 - 4\pi n_e e^2/m\omega^2$ (n_e is the charge-carrier concentration, e is the elementary charge, and m is the effective mass of the carriers). In other words, the diverging negative ε' is due to the screening of the probing electromagnetic field by supercurrents (the δ function in σ_1). The opening of the gap leads to a decrease in σ_1 at frequencies below the gap. This behavior of σ_1 and σ_2 (or ε') below T_c can also be expressed in terms of the complex refraction index $\tilde{n} = n + ik$: n diminishes, while k rises as T goes to zero. The diminishing n makes the phase shift of the wave transmitted through the film smaller and smaller.[25] This we directly see as a decrease of $x(T)$. As electrons start to condense already at T_c^{onset}, $x(T)$ begins to decrease starting at this temperature.

The measured temperature dependencies of λ for the above-mentioned frequencies are shown in Fig. 3. All curves demonstrate a very similar behavior. At low temperatures, the curves flatten. Extrapolation of $\lambda(T)$ to zero temperature gives $\lambda(0) = (1.8 \pm 0.2)$ μm. As the temperature approaches T_c, $\lambda(T)$ nearly diverges for all four frequencies (because at any nonzero frequency, σ_2 is different from zero above T_c; true divergence is not expected).

The inset of Fig. 3 shows the relative density of the superconducting condensate, $n_s = \lambda^2(0)/\lambda^2(T)$, as a function

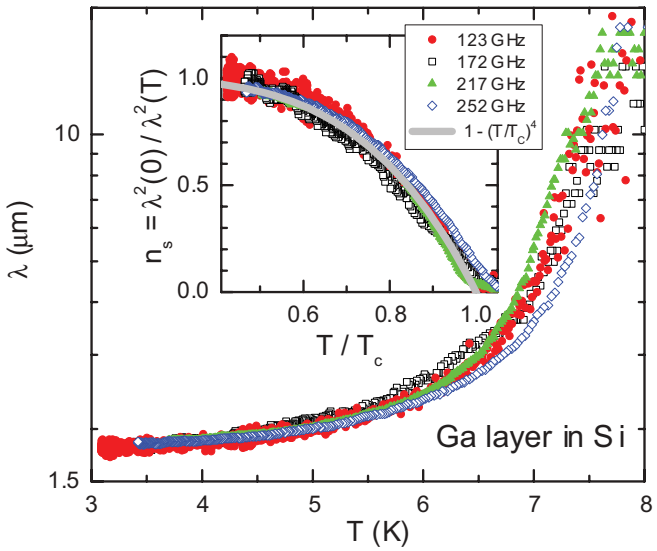

FIG. 3. (Color online) London penetration depth as a function of temperature for some frequencies. Inset: Relative density of superconducting condensate, $n_s = \lambda^2(0)/\lambda^2(T)$, as a function of temperature for the same frequencies as in the main panel. Solid line mimics the behavior expected for a fully gapped superconductor.

of temperature. All measurements basically fall onto one curve, which can be well approximated by a standard phenomenological expression used to fit the penetration depth data of conventional (fully gapped) superconductors:[15] $n_s = 1 - (T/T_c)^4$. The highest-frequency curve deviates slightly from the common trend as $T \to T_c$. We attribute this deviation to the contribution of normal-state carriers, as mentioned above (a similar behavior was observed, e.g., in Ref. 23). Our measurements are noisier at lower frequencies because the wavelength of the probing radiation at lower frequencies (123 and 172 GHz) becomes comparable to the lateral sample dimensions.

B. Frequency sweeps: Drude metal and strong-coupling *s*-wave superconductor

Normal state. Figure 4 shows (a) the as-measured transmittance, Tr(ν), and (b) the phase-shift, $\varphi(\nu)$, spectra as a function of frequency, $\nu = \omega/2\pi$ at 10 K. Since the major term of the phase shift is proportional to the frequency of the probing radiation, the phase-shift spectra are divided by frequency to eliminate the constant frequency slope. The pronounced fringes in both Tr(ν) and $\varphi(\nu)$ are due to the multiple interference within the Si substrate, which acts as a Fabry-Perot interferometer.

The scattering of the experimental data points in the spectra comes mostly from the standing-waves pattern, which is always present in continuous-wave (sub)terahertz measurements with monochromatic sources. This pattern is due to multiple reflections from all the surfaces in the optical path, e.g., from the cryostat windows and lenses. The beam path can be optimized to minimize the effect of the standing waves, but they cannot be eliminated completely.

The spectra can be well fitted by the Drude model $\sigma(\omega) = \sigma_0/(1 - i\omega\tau)$, where σ_0 is the zero-frequency limit

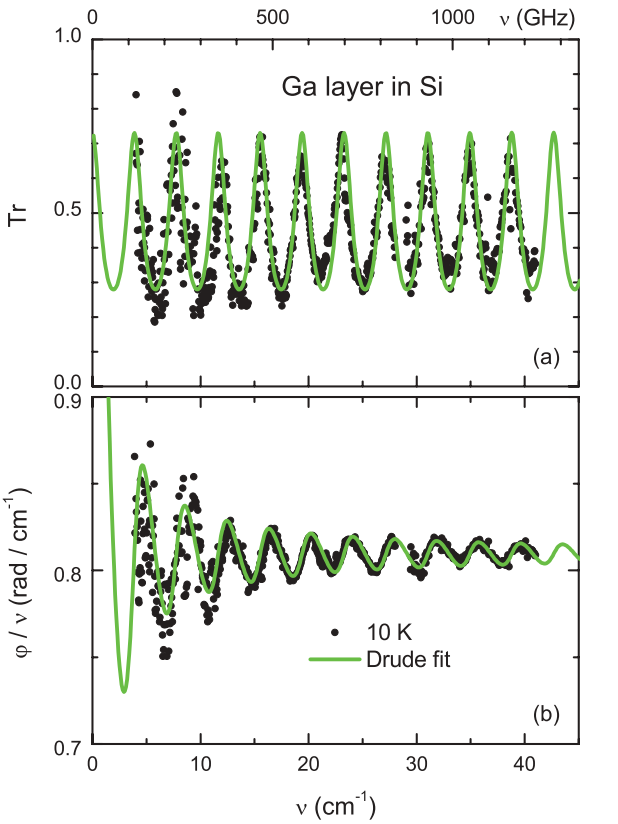

FIG. 4. (Color online) Frequency-dependent transmittance (a) and phase-shift (b) spectra of the Ga-rich layer in Si at $T = 10$ K. Solid lines show a Drude fit. The phase-shift spectra are divided by frequency for better representation.

of the conductivity and τ is the scattering time. We find $\sigma_0 = (900 \pm 150)\Omega^{-1}\,\mathrm{cm}^{-1}$ in good agreement with our dc data [$\sigma_{dc}(10\ \mathrm{K}) = 1000\ \Omega^{-1}\,\mathrm{cm}^{-1}$]. The scattering rate $\gamma = 1/(2\pi\tau)$ is above our frequency range. We can estimate $\gamma \geqslant 100\ \mathrm{cm}^{-1}$ ($\tau \leqslant 5.3 \times 10^{-14}$ s). Lower values of γ would give, at the high-frequency end of our range, an upturn in Tr(ν) larger than could be reconciled with the data. By use of the Fermi velocity for gallium, $v_F = 6 \times 10^7$ cm/s,[26] we can estimate the upper limit of the mean free path at 10 K, $\ell \leqslant 30$ nm.

At our high frequencies, we do not see a downturn of transmittance either. Such a downturn would indicate greater σ_1 values at higher frequencies and, hence, signal spatial localization of the carriers. Instead, our Drude-type conductivity proves a free-electron transport in the Ga layer. From the value of our highest measurement frequency, we can roughly estimate that no localization happens on scales of a few dozens of nanometers or larger. One cannot, of course, exclude localization effects on smaller spatial scales.

Superconducting state. The changes in the spectra related to superconductivity can best be seen in comparison with the normal-state spectra. The spectroscopic feature of the superconducting gap is supposed to be seen as a maximum in $\mathrm{Tr}_S/\mathrm{Tr}_N$ at frequencies near 2Δ.[27]

In Fig. 5(a), the ratio between the as-measured transmittances at 4 and 10 K, $\mathrm{Tr}_S/\mathrm{Tr}_N$, is shown as dots. The fringes in both the normal and the superconducting state, do not completely cancel each other. This is because of a large change

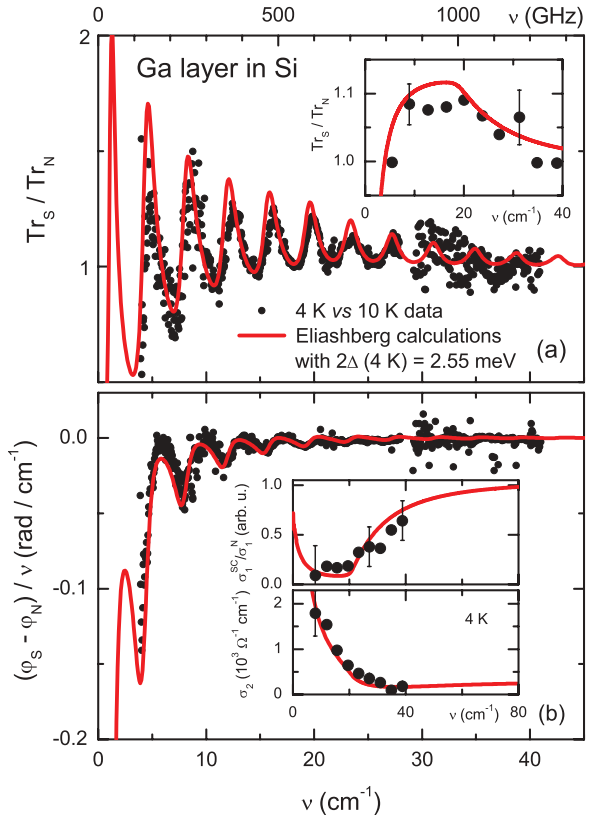

FIG. 5. (Color online) Ga-rich layer in Si in the superconducting state (4 K). On all panels, dots are measurements, lines are Eliashberg calculations with $2\Delta(4\ \mathrm{K}) = 2.55\ \mathrm{meV} = 20.6\ \mathrm{cm}^{-1}$. Main frame of panel (a): as-measured ratio between the transmittances in the superconducting, Tr_S, and normal, Tr_N, states. Main frame of panel (b): difference between the phase shifts in the superconducting (φ_S) and normal (φ_N) states divided by frequency. Inset of panel (a): $\mathrm{Tr}_S/\mathrm{Tr}_N$ obtained by averaging over each fringe together with theoretical result for a system with no multiple reflections within the substrate. Inset of panel (b): real, $\sigma_1(\nu)$, and imaginary, $\sigma_2(\nu)$, parts of the complex conductivity of the Ga-rich layer. The real part of the conductivity is divided to its normal-state value. The normal-state data used in all frames are for $T = 10$ K (Fig. 4).

of the dielectric constant of the film in the superconducting state as compared to the normal state. The fringes remaining in $\mathrm{Tr}_S/\mathrm{Tr}_N$ mask the gap feature.

In order to reveal this feature, in the inset of the panel we plot $\mathrm{Tr}_S/\mathrm{Tr}_N$ obtained by averaging the ratio over each fringe. This decreases our frequency resolution down to the distance between the fringes, but allows one to resolve the gap feature in $\mathrm{Tr}_S/\mathrm{Tr}_N$.

In Fig. 5(b) the difference between the experimental phase shifts at 4 and 10 K, $\varphi_S - \varphi_N$, is shown as dots. From the transmittance and phase-shift data in the superconductivity state, by implementing the Fresnel formulas in the same way as, e.g., in Refs. 21 and 22, we obtain the real and imaginary parts of the Ga-layer complex conductivity, shown as dots in the insets of panel (b).

In an attempt to compare experiment with theory we calculated the complex conductivity within the framework of standard s-wave Eliashberg theory.[28,29] Details of the procedure applied in these calculations are discussed elsewhere.[30] In agreement with our data on the temperature dependence of the penetration depth and with the amorphous state of Ga in our samples,[2] we assumed an isotropic s-wave gap. The Eliashberg function $\alpha^2(\omega)F(\omega)$ and the Coulomb pseudopotential $\mu^* = 0.17$ have been taken from Ref. 6. The Eliashberg function was rescaled to give T_c^{middle} keeping $\mu^\star$ unchanged. This results in a mass-enhancement factor due to electron-phonon interaction of $\lambda_{\text{el-ph}} = 1.97$ down from 2.3 as was reported by Chen *et al.*[6]

The results of these calculations are shown as solid lines in all frames of Fig. 5. The agreement between the Eliashberg calculations and the experiment is very good. Let us emphasize that we did not use any free parameters to fit the calculations to experimental points.

The zero-temperature energy gap obtained from the Eliashberg calculations is $2\Delta(0) = 2.64\ \mathrm{meV} = 21.3\ \mathrm{cm}^{-1}$; consequently, $2\Delta(0)/k_BT_c = 4.6$. As the uncertainty of the energy gap, it is reasonable to use the half-distance between the points in the insets of Fig. 5, that is $2\ \mathrm{cm}^{-1}$. This gives ± 0.5 for the uncertainty in $2\Delta(0)/k_BT_c$. The obtained value of $2\Delta(0)/k_BT_c$ is in very good agreement with the results of earlier tunneling, microwave, and infrared experiments on amorphous Ga.[6–14]

Finally, from the obtained value for $2\Delta(0)$, we can estimate the zero-temperature coherence length: $\xi_0 = \hbar v_F/\pi\Delta(0) \cong 100$ nm. Let us note that although the Ginzburg-Landau coherence length ξ^* derived from the analysis of the upper-critical-field data was found to be around 10 nm,[1] there is no contradiction with our result, because ξ^*, derived in that way, is strongly affected by the mean free path.

IV. CONCLUSIONS

Our optical data collected at terahertz frequencies on Ga-enriched layers in Si: (i) support the original observation of a superconducting transition in resistivity data[1] via the direct detection of the electromagnetic-field screening due to supercurrents; (ii) show that the London penetration depth [$\lambda(0) = 1.8\ \mu$m] and the superconducting condensate density as functions of temperature follow the typical temperature dependence expected for conventional superconductors; (iii) prove that the frequency-dependent normal-state conductivity is of Drude type (free electrons) with no signs of localization effects on length scales equal or larger than several dozens of nanometers; (iv) indicate that the upper limit of the mean free path ℓ in our sample is roughly 30 nm; and (v) allow one to estimate the size of the superconducting energy gap $2\Delta(0) = 2.64$ meV and the coherence length $\xi_0 = 100$ nm, and to conclude that our sample is a dirty ($\xi_0 > \ell$) strong-coupling ($\lambda_{\text{el-ph}} = 1.97$) s-wave superconductor with $2\Delta(0)/k_BT_c = 4.6 \pm 0.5$.

ACKNOWLEDGMENTS

Part of this work was supported by EuroMagNET II (Contract No. 228043) and by the DFG (Contract No. HE 2604/7-1).

*t.fischer@hzdr.de
†a.pronin@hzdr.de

[1]R. Skrotzki, J. Fiedler, T. Herrmannsdörfer, V. Heera, M. Voelskow, A. Mücklich, B. Schmidt, W. Skorupa, G. Gobsch, M. Helm, and J. Wosnitza, Appl. Phys. Lett. **97**, 192505 (2010).
[2]J. Fiedler, V. Heera, R. Skrotzki, T. Herrmannsdörfer, M. Voelskow, A. Mücklich, S. Oswald, B. Schmidt, W. Skorupa, G. Gobsch, J. Wosnitza, and M. Helm, Phys. Rev. B **83**, 214504 (2011).
[3]W. Buckel and R. Hilsch, Z. Phys. **138**, 109 (1954).
[4]D. G. Naugle, R. E. Glover III, and W. Moormann, Physica **55**, 250 (1971).
[5]H. M. Jaeger, D. B. Haviland, A. M. Goldman, and B. G. Orr, Phys. Rev. B **34**, 4920 (1986).
[6]T. T. Chen, J. T. Chen, J. D. Leslie, and H. J. T. Smith, Phys. Rev. Lett. **22**, 526 (1969).
[7]R. W. Cohen, B. Abeles, and G. S. Weisbarth, Phys. Rev. Lett. **18**, 336 (1967).
[8]H. Wühl, J. E. Jackson, and C. V. Briscoe, Phys. Rev. Lett. **20**, 1496 (1968).
[9]G. v. Minnigerode and J. Rothenberg, Z. Phys. **213**, 397 (1968).
[10]R. E. Harris and D. M. Ginsberg, Phys. Rev. **188**, 737 (1969).
[11]R. Meservey, P. M. Tedrow, and R. C. Bruno, Phys. Rev. **17**, 2915 (1978).
[12]J. S. Moodera and R. Meservey, Phys. Rev. **42**, 179 (1990).
[13]J. Petersen, Z. Phys. B **24**, 273 (1976).
[14]J. Goebbels and J. Hasse, Z. Phys. B **27**, 233 (1977).
[15]M. Tinkham, *Introduction to Superconductivity* (Dover, New York, 1996).
[16]D. N. Basov and T. Timusk, Rev. Mod. Phys. **77**, 721 (2005).
[17]O. S. Heavens, *Optical Properties of Thin Solid Films* (Dover, New York, 1965).
[18]A. A. Volkov, Yu. G. Goncharov, G. V. Kozlov, S. P. Lebedev, and A. M. Prokhorov, Infrared Phys. **25**, 369 (1985); A. A. Volkov, G. V. Kozlov, and A. M. Prokhorov, *ibid.* **29**, 747 (1989).
[19]G. V. Kozlov and A. A. Volkov, in *Millimeter and Submillimeter Wave Spectroscopy of Solids*, edited by G. Grüner (Springer, Berlin, 1998), p. 51.
[20]M. Dressel, N. Drichko, B. P. Gorshunov, and A. Pimenov, IEEE J. Sel. Top. Quantum Electron. **14**, 399 (2008), and references therein.
[21]A. V. Pronin, M. Dressel, A. Pimenov, A. Loidl, I. V. Roshchin, and L. H. Greene, Phys. Rev. B **57**, 14416 (1998).
[22]B. P. Gorshunov, A. V. Pronin, A. A. Volkov, H. S. Somal, D. van der Marel, B. J. Feenstra, Y. Jaccard, and J.-P. Locquet, Physica B **244**, 15 (1998).
[23]A. V. Pronin, A. Pimenov, A. Loidl, A. Tsukada, and M. Naito, Phys. Rev. B **68**, 054511 (2003).
[24]T. Fischer, A. V. Pronin, J. Wosnitza, K. Iida, F. Kurth, S. Haindl, L. Schultz, B. Holzapfel, and E. Schachinger, Phys. Rev. B **82**, 224507 (2010).
[25]From the complete Fresnel formulas (Ref. 17), one can show that the boundary contribution to the phase shift is also becoming smaller in the superconducting state as compared to the normal state.
[26]R. J. von Gutfeld and A. H. Nethercot, Phys. Rev. Lett. **18**, 855 (1967).
[27]R. E. Glover and M. Tinkham, Phys. Rev. **108**, 243 (1957).
[28]J. P. Carbotte, Rev. Mod. Phys. **62**, 1027 (1990).
[29]F. Marsiglio and J. P. Carbotte in *Superconductivity*, edited by K. H. Bennemann and J. B. Ketterson, Vol. 1 (Springer, Berlin, 2008), p. 73.
[30]T. Fischer, Ph.D. thesis, TU Dresden, 2012.